American Journal of Applied Sciences

Original Research Paper

A Model for Resolving Flow Parameters for MRI-Neuroimaging Application

Moses E. Emetere and M.L. Akinyemi

Department of Physics, Covenant University Canaan Land, P.M.B 1023, Ota, Nigeria

Article history
Received: 19-01-2015
Revised: 11-05-2015
Accepted: 19-09-2015

Corresponding Author:
Moses E. Emetere
Department of Physics,
Covenant University Canaan land, P.M.B 1023, Ota, Nigeria
Email: emetere@yahoo.com

Abstract: The functionality of recent neuroimaging using the MRI machine has generated errors which are peculiar to all kinds of MRI processes. Though hardwares are used to complement the MRI process, the problems are not completely solved due to its fundamental errors. The fundamental error is in the exclusion of molecular interaction in the ab-initio Bloch NMR. A new mathematical concept was applied to resolve the functionality problems. The Bloch NMR features and the molecular interactions were fused via a Hamiltonian process. The simulation obtained reveals the tendencies of signals to diverge. This concept was summarized via a concept known as the signal loss factor 'E'. The signal loss factor 'E' exists when spin velocity fluctuates due to compartmental boundaries in the macromolecular sites. We propose that the fundamental error-signal loss factor 'E', is a vital factor required for clinical diagnosis of cognitive impairment.

Keywords: Molecular Interactions, MR Signals, Neuro-Imaging, Cognitive Impairment

Introduction

Magnetic Resonance Imaging (MRI) is a preferred tool for clinical imaging because of its advantages which includes the absence of ionizing radiation, increased imaging flexibility and better tissue contrast. The safety in the use of MRI is commendable though it is still associated with patient claustrophobia and the presence of metal implants (George *et al*., 1990; Jobst *et al*., 1992). Aside the common application of MRI in brain imaging, it measures the brain volume, especially medial temporal lobe structures; it study the population of common brain disease e.g., Alzheimer's disease (Varma *et al*., 1999; Linn *et al*., 1995). Recently, a group of scientist discovered the possibility of diagnosing cognitive impairment using MRI via imaging sequence. Therefore, the multiplication of knowledge by scientists, engineers, mathematicians and clinicians on the MRI is boundless.

The use of fundamental mathematical concepts based on the solutions of Bloch NMR equation for MRI is definitely a novel idea (Odoh and De, 2009; Awojoyogbe *et al*., 2009; Jain *et al*., 2010; Emetere *et al*., 2014) though there are still unanswered questions on the extent of its applicability. The Bloch NMR equations are basically about magnetizations of flowing spins under given radio-frequency excitations and are dependent on the flow velocity of spins for measuring blood flow rate-velocity and volume flow rates. However, the non-inclusion of molecular markers which defines the pathology of macromolecular interactions in the original Bloch theorem restricts its research coverage. The molecular markers are most probable indicators of major micro-structural changes which occur when there is brain damage through stroke. The micro-structural changes are measured via stimulated-echo sequence (Merboldt *et al*., 1992) or pulsed-gradient spin-echo (Stejskal and Tanner, 1965). Yet the imperfections in the results obtained from the above-listed techniques (Peled *et al*., 1999; Weng *et al*., 2007; Lätt *et al*., 2007) have further expressed the need to correct mathematical exclusion of the molecular markers. Therefore the need of a modified Bloch NMR is paramount for future clinical investigations of biological systems.

An alternative approach-though not confirmed rigorously is to construct a geometric model of the microstructure of the brain. It is believed that the geometric model gives a near-perfect estimation of the MR signal from water diffusing within the brain or any part of the body. For example, the geometric model was applied to the bovine optic-nerve tissue and it corresponded with experiments (Stanisz *et al*., 1997). The main error in the geometric model is the assumption of a short gradient pulses. This error was addressed in

CHARMED model (Assaf *et al*., 2004). However, the imperfection of the CHARMED is the improper assumption which ignores the signal attenuation in geometrical content of the brain. This imperfection has been addressed (Alexander, 2008). Therefore in the bid to address the fundamental error of the Bloch NMR, more errors are made in solving for specific operation. Hence, the main objective of this paper is to theoretically resolve the fundamental error of the Bloch NMR by introducing the mathematical molecular marker into the ab-initio Bloch NMR equations and apply the results i.e. using different image and pulse sequencing to the MRI-neuroimaging. The result is essential to quantify the amount of diagnostic selection to determine the degree of cognitive impairment in patients. This model would also reduce excessive radiofrequency bombardment of sensitive region of the human brain.

Theory

Ab-Initio Operation of the Bloch NMR/MRI

The ab-initio Bloch NMR equations (Emetere, 2013a; 2014a; 2013b; 2014b; Uno and Emetere, 2012) are written as:

$$\frac{dM_x}{dt} = \Delta\omega M_y - \frac{M_x}{T_2} \tag{1}$$

$$\frac{dM_y}{dt} = -\Delta\omega M_x + \omega_1 M_z - \frac{M_y}{T_2} \tag{2}$$

$$\frac{dM_z}{dt} = -\omega_1 M_y - \frac{\left(M_z - M_o\right)}{T_1} \tag{3}$$

where, $\Delta\omega = \omega_1 - \omega_o$ is the frequency difference between Larmor frequency and the frame of reference, $\omega_1 = -\gamma B_1$ is the Rabi frequency, $\omega_o = -\gamma B_o$ is the Larmor frequency, M_x, M_y are the transverse magnetization, M_z is the longitudinal magnetization, M_o is the equilibrium magnetization.

The direct addition of any term into Equation 1-3 would certainly alter the meaning and characterization of the MR signals. Hence the incorporation of any term into the Bloch NMR may be scientifically correct if the solution of Equation 1-3 is known. Already, the solutions of steady state solutions of the Bloch equations in the rotating frame of reference are provided in (Emetere, 2014b) as:

$$M_x = \frac{\omega_1 \Delta\omega T_2^{\,2} M_0}{1 + \omega_1^2 T_1 T_2 - \Delta\omega^2 T_2^{\,2}} \tag{4}$$

$$M_y = \frac{\omega_1 T_2 M_o}{1 + \omega_1^2 T_1 T_2 - \Delta\omega^2 T_2^{\,2}} \tag{5}$$

$$M_z = \frac{(1 + \Delta\omega^2 T_2^{\,2}) M_o}{1 + \omega_1^2 T_1 T_2 - \Delta\omega^2 T_2^{\,2}} \tag{6}$$

Further assumption to Equation 1-3 defines the type of MRI i.e., diffusion MRI, continuous wave, functional MRI, Bloch flow MRI, diffusion-tensor MRI.

Materials and Methods

Resolution of the Bloch NMR/MRI for Biological Systems

The inclusion of the molecular dynamic to the Bloch NMR for adequate application to clinical diagnosis shall be the focus in this section. The molecular dynamics includes the macromolecular interaction which can be evidently seen in the variation of relaxation times between tissues due to compartmental boundaries and other molecular obstacles.

In order to account for the molecular dynamics of the Bloch approach in a Continuous Wave Nuclear Magnetic Resonance (CW NMR) flow equation, we propose a generic Hamiltonian to incorporate both the Bloch NMR and Molecular dynamics:

$$H_T = H_{Bloch} + H_{Molecular} \tag{7}$$

H_{Bloch} is represented by the flow magnetization equation derived by (Awojoyogbe *et al*., 2009):

$$H_{Bloch} = v^2 \frac{\partial^2 M_y}{\partial x^2} + v\left(\frac{1}{T_1} + \frac{1}{T_2}\right)\frac{\partial M_y}{\partial x} + \left(\frac{1}{T_1 T_2} + \gamma^2 B_1^{\,2}\right) M_y - \frac{\gamma B_1 M_o}{T_1} \tag{8}$$

$$H_{Molecular} = \frac{\partial E}{\partial x_i}\frac{\partial E}{\partial x_j} \tag{9}$$

All parameters maintain its original interpretations. Along the i^{th} site, the elastic model for macromolecular interactions is predominant. Therefore, $E = \sum_i^N V(x_i) + \sum_{i=2}^N \frac{1}{2} k\left(x_i - x_{i-1}\right)^2$, Along j^{th} site the energy E coincide with the energy levels worked out by (Emetere, 2013a) for NMR studies. $V(x_i)$ is the potential across compartmental boundaries. This factor is important for analyzing both microscopic and macroscopic imaging techniques:

$$E = 1 - m.\omega_1 M_y \mathrm{T}_1 \tag{10}$$

where, $\omega_1 = -\gamma B_1$ the Rabi frequency, μ is the magnetic moment, M_y is the applied transverse magnetization and T_1 is the spin-lattice relaxation time. Assume

$m.\omega_1 M_y T_1 >> 1$, Equation 9 can be further spitted into Equation 11 and 12. This method is usually done in the matrix form:

$$\frac{\partial E}{\partial x_j} = \mu.\omega_1 \mathrm{T}_1 \frac{\partial M_y}{\partial x} \tag{11}$$

$$\frac{\partial E}{\partial x_i} = \sum_i^N \frac{\partial V(x_i)}{\partial x} + \sum_{i=2}^N \frac{1}{2} k\left(x_i - x_{i-1}\right)^2 \tag{12}$$

Therefore, the total Hamiltonian can be written as:

$$\begin{aligned} H_T &= v^2 \frac{\partial^2 M_y}{\partial x^2} + v\left(\frac{1}{T_1} + \frac{1}{T_2} + \mu.\omega_1 \mathrm{T}_1\right)\frac{\partial M_y}{\partial x} \\ &+ \sum_i^N \frac{\partial V(x_i)}{\partial x} + \left(\frac{1}{T_1 T_2} + \gamma^2 B_1^{\,2}\right) M_y - \frac{\gamma B_1 M_o}{T_1} \end{aligned} \tag{13}$$

We assume $\sum_{i=2}^N \frac{1}{2} k\left(x_i - x_{i-1}\right)^2 = 0$ for the gray-white matter of the brain. Applying the Schrödinger i.e., $H\psi = E\psi$, equation (Jain *et al*., 2010) transforms into:

$$\begin{aligned} &v^2 M_y \frac{\partial^2 \psi}{\partial x^2} + [v\left(\frac{1}{T_1} + \frac{1}{T_2} + \mu.\omega_1 \mathrm{T}_1\right) M_y + \sum_i^N V(x_i)]\frac{\partial \psi}{\partial x} \\ &+ \left[\left(\frac{1}{T_1 T_2} + \gamma^2 B_1^{\,2}\right) M_y - E - \frac{\gamma B_1 M_o}{T_1}\right]\psi = 0 \end{aligned} \tag{14}$$

ψ had been calculated by (Emetere, 2013a) for NMR studies. It is summarized as $\psi = Aexp(i\omega t)$. In order to analyze the time-independent domain, we place $t = \frac{xr}{\omega}$, where x is the circumference of the base sector of the cone, r is the radial component. Therefore:

$$\psi = Aexp(ixr) \tag{15}$$

Substituting Equation 15 into Equation 8 yields two sets of governing equations:

$$v^2 r^2 M_y + \left(\frac{1}{T_1 T_2} + \gamma^2 B_1^{\,2}\right) M_y - E - \frac{\gamma B_1 M_o}{T_1} = 0 \tag{16}$$

$$v\left(\frac{1}{T_1} + \frac{1}{T_2} + \mu.\omega_1 \mathrm{T}_1\right) M_y + \sum_i^N V(x_i) = 0 \tag{17}$$

The governing equations yield the following solutions:

$$M_y = \frac{ET_1 T_2 + \gamma B_1 M_o T_2}{v^2 r^2 T_1 T_2 + 1 + \gamma^2 B_1^{\,2} T_1 T_2)} \tag{18}$$

$$M_y = \frac{T_1 T_2 \sum_i^N V(x_i)}{(\tau + \mu.\omega_1 T_1^{\,2} T_2) v} \tag{19}$$

where, $\tau = T_1 + T_2$. If $v^2 r^2 T_1 T_2 << 1$ and $ET_1 T_2 << 1$, the Equation 18 yields:

$$M_y = \frac{\gamma B_1 T_2 M_o}{1 + \gamma^2 B_1^{\,2} T_1 T_2} \tag{20}$$

Equation 20 is the exact solution of the CW NMR and is expressed in the laboratory frame as:

$$M_{xo} = \frac{-\sin\sin(\omega t)\gamma B_1 T_2 M_o}{1 + \gamma^2 B_1^{\,2} T_1 T_2} \tag{21}$$

$$M_{yo} = \frac{\cos(\omega t)\gamma B_1 T_2 M_o}{1 + \gamma^2 B_1^{\,2} T_1 T_2} \tag{22}$$

This result had been reported by numerous researchers (Odoh and De, 2009) i.e., showing the validity of our approach. Also, if $\mu.\omega_1 T_1^{\,2} T_2 \gg \tau$, Equation 19 yields a new exact solution of the CW NMR i.e.:

$$M_y = \frac{\sum_i^N V(x_i)}{\mu.\omega_1 T_1 v} \tag{23}$$

The exact solution of CW NMR in a laboratory frame can also be written as:

$$M_{xo} = \frac{-\sin(\omega t)\sum_i^N V(x_i)}{\mu.\omega_1 T_1 v} \tag{24}$$

$$M_{yo} = \frac{\cos(\omega t)\sum_i^N V(x_i)}{\mu.\omega_1 T_1 v} \tag{25}$$

Therefore, the flow velocity of the spin can be calculated in its raw form as:

$$v = \frac{\left(1 + \gamma^2 B_1^{\,2} T_1 T_2\right)\sum_i^N V(x_i)}{\mu.\omega_1 \gamma B_1 M_o T_1 T_2} \tag{26}$$

If $\gamma^2 B_1^{\,2} T_1 T_2 \gg 1$:

$$v = \frac{\gamma B_1 \sum_i^N V(x_i)}{\mu.\omega_1 M_o} \tag{27}$$

Therefore the flow velocity of the spin in the laboratory frame can be written as:

$$v_{xo} = \frac{-\sin(\omega t)\gamma B_1 \sum_i^N V(x_i)}{\mu.\omega_1 M_o} \tag{28}$$

$$v_{yo} = \frac{\cos(\omega t)\gamma B_1 \sum_i^N V(x_i)}{\mu.\omega_1 M_o} \tag{29}$$

In line with Helsinki declaration, parts of the results have been discussed at the IWBBIO 2014 conference.

Results

In practical application for tissue, the T_1 is in the range of 3 to 80 ms (Bloom *et al*., 1986; Peemoeller *et al*., 1982), the selective and nonselective pulse is in the range 40 to 200 MHz (Sobol *et al*., 1986), E in Equation 18 is the energy required to optimize signal-to-noise ratios to enhance better final images (Lee and Riederer, 1987). The field strength required is within the range 1.5 to 4.0 T (Jezzard and Balaban, 1995) though voxels of grayish-white matter are usually of lesser field strength say 1.5 to 2.0 T.

In order to compute the sections of the brain, we assume four sections with its peculiar compartmental boundaries as shown in the Fig. 1 i.e., skull, blood, water and grayish-white matter. We proposed varying potentials V(x) for the four sections with respect to their physical properties i.e., solid, liquid and aqueous. Basically, the apparent diffusivity of the brain gray matter is largely independent of the orientation of the tissue (i.e., isotropic) while the diffusivity of skeletal, cardiac muscle and white matter of the brain depends upon the orientation of the tissue. Blood and water are liquids with different viscosity; their values were proposed as shown in Equation 30. From the trend of the general flow parameters, it is scientific (when the brain isotropic) to assume that the potential across liquid takes the partial quadratic form as shown below. The potential across the skull was assumed to be unity though experimentally, it varies in individual because of bone density. The gray-white tissues (which include cortical grey matter, subcortical white matter) of the brain were assumed to possess an exponential potential due to its macromolecular interactions:

$$V(x) = \begin{cases} x_s : x \\ x_b : x^2 + x \\ x_w : \frac{x^2}{16} + \frac{x}{4} \\ x_g : \exp(xr) \end{cases} \tag{30}$$

In this model, $V(x_i)$ is the theoretical slice selection technique that defines the arterial spin labeling timing, arterial transit delay and the apparent decay time of the signal. Depending on the part of the body, $V(x_i)$ could be modeled using polynomial expansion schemes e.g., Boubaker, Chebyshev, Legendre, Bessel. In this study, we adopted Equation 30 to magnify the abnormal signals associated to diverse process errors during neuroimaging.

The spin velocity for different neurological examination is shown in the Fig. 2. The doted green line signifies an abnormal Headache in patients, the dotted black line signifies an abnormal neurological examination and the red dotted line signifies the existence of neurological symptoms. The spin velocity at each case is affected by the abnormal expansion of the blood vessels in the brain i.e., endothelium. Therefore, a sudden increase in measured speed signifies the presence of neurological symptoms.

The effects of the nominal tip angle of various RF excitations on the spin flow was investigated (using $\frac{\pi}{2}, \frac{\pi}{3}, \frac{\pi}{6}$) as shown in Fig. 3-5. At this point the transverse magnetization is believed to be constant.

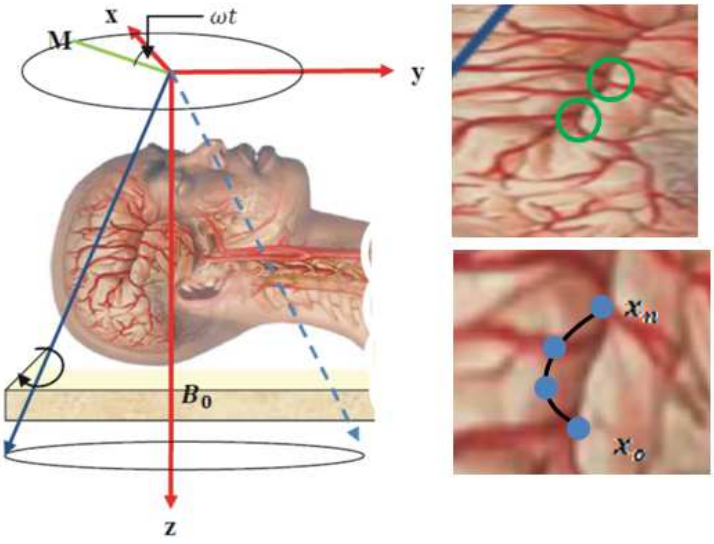

Fig. 1. Neuroimaging of the brain (Retrieved on 2/11/13, http://health.shorehealth.org/imagepages/19224.htm)

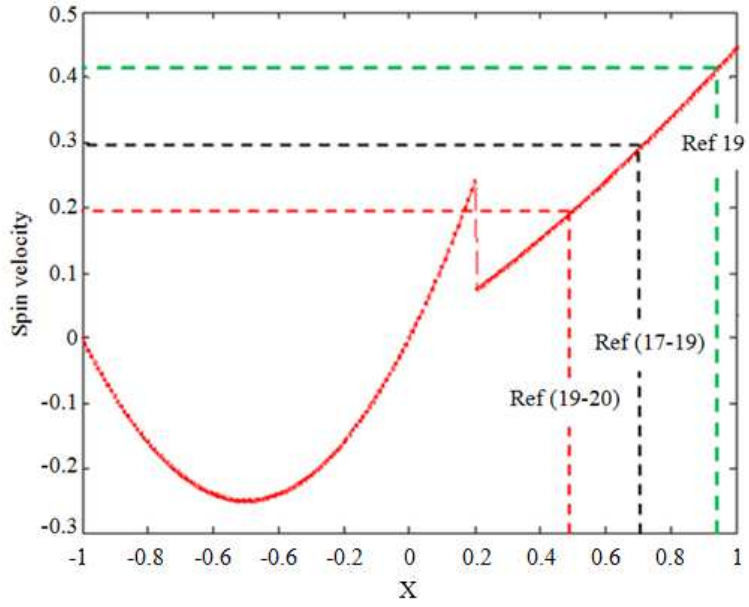

Fig. 2. Signaling interpretation of experimental data

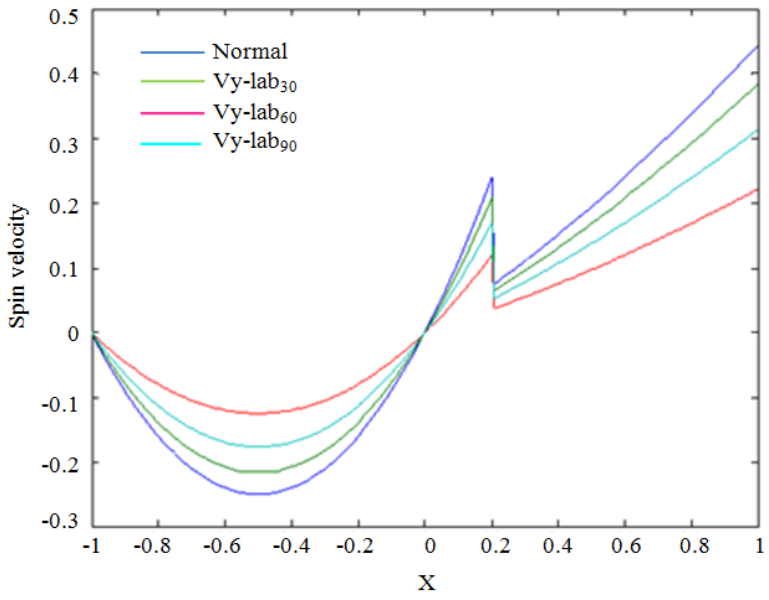

Fig. 3. Signaling in a M_{yo} laboratory frame

The first RF excitation occurs when the nominal tip angle is $\pi/3$. This idea is quite different from the sequence suggested in (Wladyslaw, 1989). The positive (Fig. 4) and negative (Fig. 5) velocity in a laboratory frame was also investigated. While the negative spin velocity follows the normal rf pulse pattern, the positive spin velocity opens up the reality of signal loss in the Bloch flow systems e.g., stenotic flow (Siegel Jr. *et al*., 1997).

One of the objectives of this paper is to resolve the signal loss which is majorly caused by fluctuating velocity. As can be seen in Fig. 6, when the spin velocity flows across the x-axis of the brain, its transmission through the compartmental boundaries of the gray-white matter of the brain experiences an internal deviation which increases the size of the spin packet from $\gamma B_1 M_o$ to $(E+\gamma B_1 M_o)$. This event produces blurred images which are corrected by the use of digital signal processors. In reality, the additional factor 'E' ought not to be screened away but harvested in order to measure more complex problem like cognitive impairment. For example, we propose that the farther deviated a scattered signal from its originating packet (or higher value of 'E'), the greater the cognitive impairment.

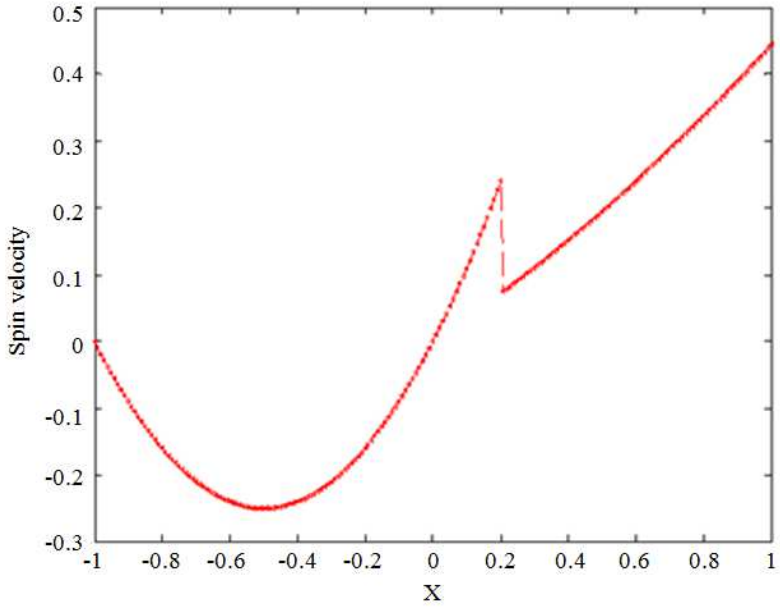

Fig. 4. Signaling in a M_{xo} laboratory frame

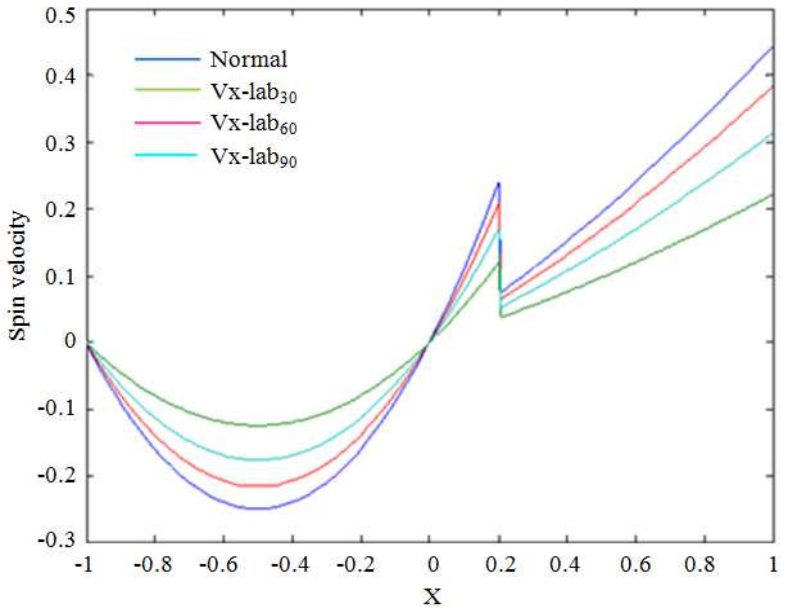

Fig. 5. Signaling in a recoiled M_{xo} laboratory frame

Figure 6 can be further expressed in a more practical term as shown in Fig. 7. For example, if there is a deformation represented as the blue shape.

When the RF signal is applied, the spin velocity shown travels-divergently in a uniform path as shown in Fig. 7a. This is because the endothelial cells (which are the lining that separates the capillaries in the brain from the brain tissue) are ignored in the ab-inito Bloch-from which multi MRI processes emanates. The errors in these kind of MRI process generates errors from the endothelial cells-lining the walls of blood vessels contain glucose; gray-matter volume and density; white-matter volume and density; neurochemical receptors. Scientists have adopted few hardware to reduce MRI operational errors e.g., the Voxel-Based Morphometry (VBM) method (Good *et al*., 2001; Emetere *et al*., 2014) are used for analyzing gray-matter density. From the explanation of Fig. 6, if 'E' is properly harnessed, it converge signals more specifically to the deformation (as shown in Fig. 7b).

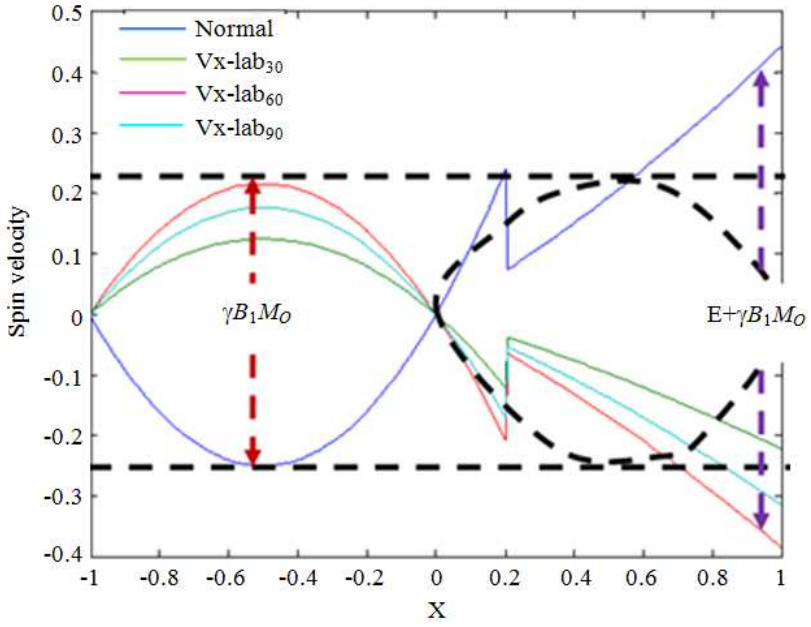

Fig. 6. Signaling abnormities in neuroimaging

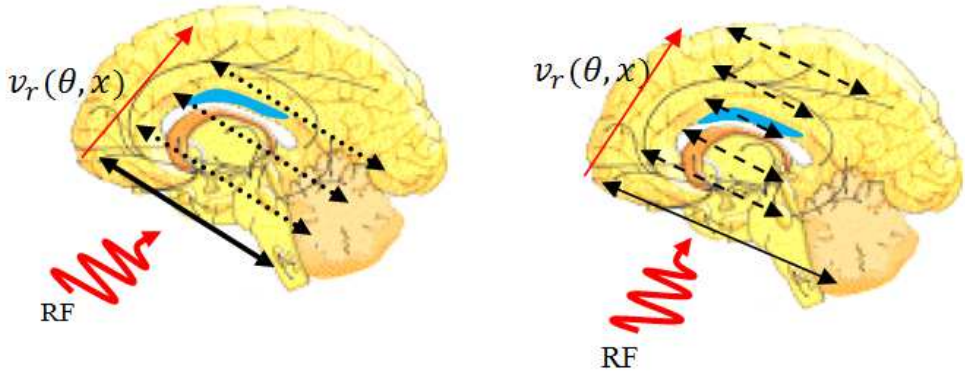

(a) (b)

Fig. 7. RF pulse sequence on the brain deformation (blue shape), (a) the normal sequence; (b) the converging sequence due to molecular markers

The molecular interaction enables the spin velocity transverse more specifically towards the deformation in the brain and produces clear picture in either the short or long run.

Conclusion

The additive functionality to the Bloch NMR flow equations has been improved upon-the possibilities in the MRI-neuroimaging to detect with accuracy more complex problems in neurological examination. The signal loss due to fluctuating velocity as it transmits through compartmental molecular boundaries is also essential for higher diagnostic selection to determine the degree of cognitive impairment in patient. The introduction of the potential across segregated states of matter within the living tissue is a leeway for introducing higher mathematical techniques into the solutions of Bloch NMR equation for MRI applications.

Acknowledgement

The author appreciates the partial sponsorship of Covenant University. The author declares that there is no competing or financial interest.

Author's Contributions

Moses Emetere Moses: Write-up and research design.

M.L. Akinyemi: Proof-reading and facilitating research funding.

Ethics

This article is original and contains unpublished material. The corresponding author confirms that all of the other authors have read and approved the manuscript and no ethical issues involved.

Reference

Alexander, D.C., 2008. A general framework for experiment design in diffusion MRI and its application in measuring direct tissue-microstructure features. Magnetic Resonance Med., 60: 439-448. DOI: 10.1002/mrm.21646

Assaf, Y., R.Z. Freidlin, G.K. Rohde and P.J. Basser, 2004. New modeling and experimental framework to characterize hindered and restricted water diffusion in brain white matter. Magn. Reson. Med., 52: 965-978. DOI: 10.1002/mrm.20274

Awojoyogbe, O.B., M. Dada, O.P. Faromika, O.F. Moses and I.A. Fuwape, 2009. Polynomial solutions of Bloch NMR flow equations for classical and quantum mechanical analysis of fluid flow in porous media. Open Magnetic Resonance J., 2: 46-56. DOI: 10.2174/1874769800902010046

Bloom, M., K.T. Holmes, C.E. Mountford and P.G. Williams, 1986. Complete proton magnetic resonance in whole cells. Magn. Reson., 69: 73-91. DOI: 10.1016/0022-2364(86)90219-2

Emetere, M.E., 2013a. Mathematical modeling of Bloch NMR to solve the Schrodinger time dependent equation. Afr. Rev. Phys., 8: 65-68.

Emetere, M.E., 2013b. Mathematical modeling of Bloch NMR to explain the Rashba energy features. Sci. Res. World J. Condensed Matter Phys., 3: 87-94.

Emetere, M.E., 2014a. Mathematical modeling of Bloch NMR to solve a three dimensional-Schrodinger time dependent equation. Applied Math. Sci., 8: 2753-2762.

Emetere, M.E., 2014b. Characteristic significance of magnetic relaxations on copper oxide thin film using the Bloch NMR. Surface Rev. Lett., 21: 1450075-1450084. DOI: 10.1142/S0218625X14500759

Emetere, M.E., O.B. Awojoyogbe, U.E. Uno, K.U. Isah and O.M. Dada, 2014. Resolving the enhanced flow parameters for an In-depth analysis of the MRI-neuroimaging. Proceedings of the IWBBIO Apr. 7-9, Granada, pp: 810-819.

George, A.E., M.J. de Leon, L.A. Stylopoulos, J. Miller and A. Kluger *et al*., 1990. CT diagnostic features of Alzheimer disease: Importance of the choroidal/hippocampal fissure complex. Am. J. Neuroradiol., 11: 101-107. PMID: 2105589

Good, C.D., I.S. Johnsrude, J. Ashburner, R.N.A. Henson and K.J. Friston *et al*., 2001. A voxel-based morphometric study of ageing in 465 normal adult human brains. NeuroImage, 14: 21-36. DOI: 10.1006/nimg.2001.0786

Jain, V., M.C. Langham and F.W. Wehrli, 2010. MRI estimation of global brain oxygen consumption rate. J. Cerebral Blood Flow Metabolism, 30: 1598-1607. DOI: 10.1038/jcbfm.2010.49

Jezzard, P. and R.S. Balaban, 1995. Correction for geometric distortion in echo planar images from B0 field variations. Magn. Reson. Med., 34: 65-73. DOI: 10.1002/mrm.1910340111

Jobst, K.A., A.D. Smith, M. Szatmari, A. Molyneux and M.E. Esiri *et al*., 1992. Detection in life of confirmed Alzheimer's disease using a simple measurement of medial temporal lobe atrophy by computed tomography. Lancet, 340: 1179-1183. PMID: 1359259

Lätt, J., M. Nilsson, C. Malmborg, H. Rosquist and R. Wirestam *et al*., 2007. Accuracy of *q*-space related parameters in MRI: Simulations and phantom measurements. IEEE Trans. Med. Imag., 26: 1437-1447. DOI: 10.1109/TMI.2007.907278

Lee, J.N. and S.J. Riederer, 1987. The contrast-to-noise in relaxation time, synthetic and weighted-sum MR images. Magn. Reson. Med., 5: 13-22. DOI: 10.1002/mrm.1910050103

Linn, R.T., P.A. Wolf, D.L. Bachman, J.E. Knoefel and J.L. Cobb *et al*., 1995. The 'preclinical phase' of probable Alzheimer's disease. A 13-year prospective study of the Framingham cohort. Arch Neurol., 52: 485-490. DOI: 10.1001/archneur.1995.00540290075020

Merboldt, K.D., W. Hanicke and J. Frahm, 1992. Diffusion imaging using stimulated echoes. Magn. Reson. Med., 19: 233-239. DOI: 10.1002/mrm.1910190208

Odoh, E.O. and D.K. De, 2009. Application of nuclear magnetic resonance imaging in blood flow estimation. Afr. Phys. Rev.. 3: 65-74.

Peemoeller, H., R.K. Shenoy, M.M. Pintar, D.W. Kydon and W.R. Inch, 1982. Improved characterization of healthy and malignant tissue by NMR line-shape relaxation correlations. Biophys. J., 38: 271-295. DOI: 10.1016/S0006-3495(82)84558-X

Peled, S., D.G. Cory, S.A. Raymond, D.A. Kirschner and F.A. Jolesz, 1999. Water diffusion, T_2 and compartmentation in frog sciatic nerve. Magn. Reson. Med., 42: 911-918. DOI: 10.1002/(SICI)1522-2594(199911)42:5<911::AID-MRM11>3.0.CO;2-J

Siegel Jr. J., J. Oshinski, R. Pettigrew and D. Ku, 1997. Computational simulation of turbulent signal loss in 2D time-of-flight magnetic resonance angiograms. Magn. Reson. Med., 37: 609-614. DOI: 10.1002/mrm.1910370421

Sobol, W.T., I.G. Cameron, W.R. Inch and M.M. Pintar, 1986. Modeling of proton spin relaxation in muscle tissue using nuclear magnetic resonance spin grouping and exchange analysis. Biophys. J., 50: 181-191. DOI: 10.1016/S0006-3495(86)83450-6

Stanisz, G.J., A. Szafer, G.A. Wright and M. Henkelman, 1997. An analytical model of restricted diffusion in bovine optic nerve. Magn. Reson. Med., 37: 103-111. DOI: 10.1002/mrm.1910370115

Stejskal, E.O. and T.E. Tanner, 1965. Spin diffusion measurements: Spin echoes in the presence of a time-dependent field gradient. J. Chem. Phys., 42: 288-292. DOI: 10.1063/1.1695690

Uno, U.E. and M.E. Emetere, 2012. Analysis of the high temperature superconducting magnetic penetration depth using the Bloch NMR equations. Global Eng. Technol. Rev., 2: 14-21.

Varma, A.R., J.S. Snowden, J.J. Lloyd, P.R. Talbot and D.M. Mann *et al*., 1999. Evaluation of the NINCDS-ADRDA criteria in the differentiation of Alzheimer's disease and frontotemporal dementia. J. Neurol. Neurosurg. Psychiatry, 66: 184-188. PMID: 10071097

Weng, J.C., J.H. Chen, L.W. Kuo, V.J. Wedeen and W.Y. Tseng, 2007. Maturationdependent microstructure length scale in corpus callosum of fixed rat brain by magnetic resonance diffusion-diffraction. Magn. Reson. Imag, 25: 78-86. DOI: 10.1016/j.mri.2006.08.018

Wladyslaw, T.S., 1989. Medical applications of NMR. Bull. Magn. Reson., 11: 69-85.